Co-Deposition and Poisoning of Chromium and Sulfur Contaminants on $La_{0.6}Sr_{0.4}Co_{0.2}Fe_{0.8}O_{3-\delta}$ Cathodes of Solid Oxide Fuel Cells

Cheng Cheng Wang,[a] Kane O'Donnell,[b] Li Jian,[c] and San Ping Jiang[a,z]

[a]*Fuels and Energy Technology Institute & Department of Chemical Engineering, Curtin University, Perth, WA 6102, Australia*
[b]*Department of Imaging and Applied Physics, Curtin University, Perth, WA 6102, Australia*
[c]*Center for Fuel Cell Innovation, School of Materials Science and Engineering, State Key Laboratory of Materials Processing and Die & Mould Technology, Huazhong University of Science and Technology, Wuhan 430074, People's Republic of China*

The presence of both chromium and sulfur (Cr/S) contaminants on the microstructure and electrocatalytic activity properties of $La_{0.6}Sr_{0.4}Co_{0.2}Fe_{0.8}O_{3-\delta}$ (LSCF) electrodes of solid oxide fuel cells (SOFCs) is studied, using Confocal laser Raman spectroscopy, XRD, scanning electron microscopy, X-ray photoelectron spectroscopy (XPS) and electrical conductivity relaxation (ECR) methods. LSCF dense bar samples were heat treated in the presence of Cr_2O_3 and 20 ppm SO_2 and in the temperature range of 600–900°C. The deposition and reaction products between LSCF and Cr/S depend on the temperature: $SrCrO_4$ only forms on LSCF samples at 900°C and 800°C, while formation of $SrSO_4$ phase occurs at all temperatures studied. The results indicate that sulfur shows a higher activity with LSCF, as compared to gaseous Cr species. Segregated SrO is more likely to react with gaseous Cr species at higher temperatures, however, reaction with SO_2 is more pronounced at lower temperatures, forming $SrSO_4$. ECR results indicate that co-deposition of Cr and sulfur significantly deteriorates the surface exchange and diffusion processes for the O_2 reduction reaction on LSCF electrodes.

 [DOI: 10.1149/2.0231506jes]

Manuscript submitted January 12, 2015; revised manuscript received February 13, 2015. Published February 24, 2015.

The durability of a solid oxide fuel cell (SOFC) is critically related to the degradation behavior of its cathodes such as $La_{0.8}Sr_{0.2}MnO_3$ (LSM) and $La_{0.6}Sr_{0.4}Co_{0.2}Fe_{0.8}O_{3-\delta}$ (LSCF) in the presence of impurity species such as chromium from the chromia-forming interconnect, silica, boron and volatile alkaline elements from the glass seals sealant and sulfur from air.[1–8] Among them, gaseous chromium species vaporized from the chromium oxide scale of chromia-forming metallic interconnect are probably the most investigated contaminants affecting the performance of SOFCs' cathodes. The mechanism and process of the deposition and poisoning of chromium species at the cathodes of SOFCs have been extensively investigated, including LSM,[9–11] LSCF[12] and $Ba_{0.5}Sr_{0.5}Co_{0.8}Fe_{0.2}O_{3-\delta}$ (BSCF).[13] In the case of LSCF electrodes, deposition of Cr species preferentially take place on the surface of the LSCF electrode, resulted from the interaction between the segregated SrO and gaseous Cr species.[14,15] Both the humidity in the air stream and operation temperature have a significant effect on the Cr deposition.[16] Cr deposition decreases significantly with the decrease of temperature, most likely due to the reduced Sr segregation as well as the decrease of the partial pressure of gaseous Cr species at reduced temperatures.[17]

The sulfur in the form of SO_2 or H_2S in the air stream is another important contaminant affecting the performance stability of SOFC cathodes. SO_2 content in air can be in the range of 10–340 $\mu g\ m^{-3}$ (3.5×10^{-3} – 0.12 ppm) in cities.[18] Despite the low concentration of SO_2, sulfur in the air stream can accumulate at the cathodes of SOFC cells, degrading the performance.[5] Wang et al.[19] studied the polarization performance behavior of LSCF in the presence of 0.1 ppm SO_2 and observed two-stages of performance degradation. A degradation mechanism based on the occupation of SO_2 in the oxide ion vacancies and subsequent formation of SO_3^{2-} and $SrSO_4$ was proposed for the irreversible poisoning effect of SO_2. Liu et al.[20] showed that the performance of cells with a LSCF electrode becomes unstable in the presence of 1 ppm SO_2 and drops significantly when the SO_2 concentration increases to 20 ppm. The performance degradation is most likely due to the poisoning of SO_2 and the formation of $SrSO_4$. We studied recently the sulfur deposition and poisoning mechanism of LSCF electrodes and found that sulfur (i.e., SO_2) reacts with LSCF, primarily forming $SrSO_4$ phase at high temperatures (i.e., $\geq$700°C) and SrS at low temperatures (i.e. <700°C).[21] Sulfur deposition shows a strong dependence on the temperature and is most severe at temperatures around 700°C, indicating that sulfur deposition and poisoning on LSCF are closely related to the operating temperature of fuel cells.[21]

In SOFC stack operation conditions, both chromium and sulfur source exists. Horita et al.[5] studied the effect of impurities on the performance stability of the flatten tubular SOFC stack and found that the concentrations of contaminants like Cr, Si and S increase with the operation time. Schuler et al.[4] studied the air side contaminants under SOFC stack configuration. Post-analyses of the cells showed that performance degradation is mainly due to the contaminants at the cathode originated from the upstream of the cell. Further studies[22] on the Ni-YSZ anode-supported thin YSZ electrolyte cells with the LSM/YSZ composite cathodes showed the formation of $Sr(Cr,S)O_4$ in the LSM/YSZ composite cathode layer after tested for 1900 h at 800°C, indicating the presence of Cr and S contaminants. However, there appear no reports on the deposition and poisoning of LSCF cathodes in the presence of both Cr and S contaminants.

In this study, the presence of both Cr and S contaminants on the microstructure and surface diffusion properties of LSCF cathode materials is investigated from 900 to 600°C on LSCF dense bar samples in air. The results indicate that sulfur deposition and poisoning effect is more dominant as compared to the chromium particularly at temperatures $\leq$700°C under the conditions of this study. Electrical conductivity relaxation (ECR) results also indicate that Cr and S poisoning strongly deteriorate the surface exchange and diffusion processes for the O_2 reduction reaction on LSCF electrodes.

Experimental

$La_{0.6}Sr_{0.4}Co_{0.2}Fe_{0.8}O_{3-\delta}$ powders (LSCF, Fuel Cell Materials) were pressed into a rectangular bar at 300 MPa, and then fired at 1350°C for 5 h in air to form dense LSCF bar samples. The size of the sintered samples is 25 mm × 6.6 mm × 0.62 mm. The LSCF bar samples were heat treated at temperatures from 900°C to 600°C in the presence and absence of Cr_2O_3 and 20 ppm SO_2 (SO_2 in N_2, BOC

[z]E-mail: s.jiang@curtin.edu.au

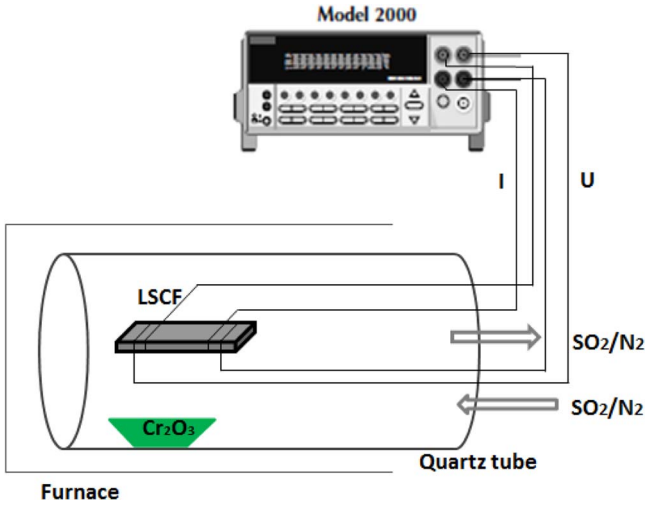

Figure 1. Schematic diagram of LSCF bar samples for the ECR test in the presence of Cr_2O_3 and 20 ppm SO_2.

Ltd.). Cr_2O_3 was used as the source of gaseous Cr species and flow rate of SO_2 was 20 sccm. The conductivity relaxation profiles of LSCF bar samples were measured by a standard four-probe method using a measurement system consisting of a Digital Multimeter (Keithley 2001) equipped with a computer and a program written using the LABVIEW 8.5 software. Pt wires were used as the leads, which were attached to the Pt electrode using Pt paste. The measurements were carried out at a selected temperature of 900°C with oxygen partial pressure changing from 0.05 bar to 0.21 bar in the presence of Cr and S, respectively, and in the presence of both Cr and S (or Cr/S). The electrical conductivity data of the bar samples were recorded as a function of exposed time and the experimental data were fitted to the theoretical equations[23] to calculate the oxygen surface exchange coefficients, k_{chem}. The experimental setup for the ECR measurement and co-deposition of Cr and S of LSCF bar samples is shown in Figure 1.

XRD (D8 Advance, Bruker, Germany) and Confocal laser Raman spectroscopy (WITec GmbH, Ulm Germany) techniques were used to examine the phase composition of LSCF bar samples. The morphology and microstructure of the bar samples after the heat-treatment at different temperatures in the presence of Cr and S species were studied by scanning electron microscopy (SEM) and energy dispersive spectroscopy using a Zesis EVO with 20 keV. X-ray photoelectron spectroscopy (XPS) was performed using a Kratos AXIS Ultra DLD instrument using monochromated Al Kα X-rays (energy 1486.7 eV). A pass energy of 40 eV was used for the core level spectra. The binding energy (BE) scale was calibrated with respect to the adventitious carbon component of the C 1s peak fixed at 284.8 eV. Background subtraction and peak fitting were performed with Casa XPS.

Results and Discussion

XRD and microstructure.— Figure 2 shows the XRD pattern of as-prepared LSCF as well as LSCF bar samples after heat-treatment in the presence of Cr_2O_3 and 20 ppm SO_2 (or Cr+S) at different temperatures for 48 h. The as-prepared LSCF shows typically XRD patterns associated with rhombohedral perovskite structure (curve a, Fig. 2). Diffraction peak at $2\theta = 29°$ was observed for LSCF samples heat treated at 900°C and 800°C and can be identified as the formation of $SrCrO_4$ phase,[24] while for the sample heat treated at 700°C and 600°C, peak at $2\theta = 27°$ associated with the formation of $SrSO_4$[25] was detected. The formation of $SrSO_4$ phase is also observed on LSCF samples after the heat-treatment in the presence of SO_2 when the temperature is equal to or lower than 700°C.[17]

Figure 3 is the SEM micrographs of the LSCF surfaces after the heat-treatment in the presence of Cr_2O_3 and 20 ppm SO_2 in air at

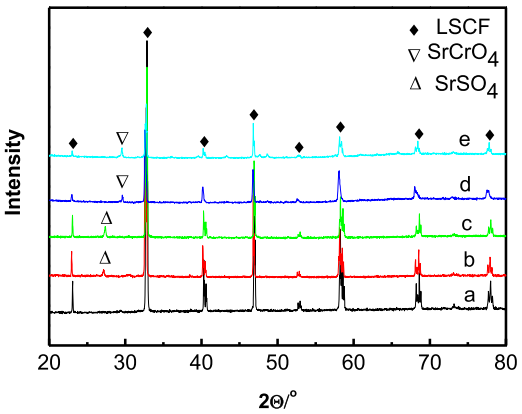

Figure 2. XRD diffraction patterns of as-prepared LSCF and LSCF bar samples after heat-treatment in the presence of Cr_2O_3 and 20 ppm SO_2 at different temperatures for 48 h. a) as-prepared, b) 600°C, c) 700°C, d) 800°C, e) 900°C.

different temperatures for 48 h. For the purpose of comparison, the SEM micrographs of LSCF surface after the heat-treatment in the presence of Cr_2O_3 or 20 ppm SO_2 in air at different temperatures[17,21] were also shown in the figure. There are significant increases in both the size and number of deposits on the LSCF surface. In the case of LSCF samples treated at 900°C in the presence of Cr_2O_3 only, the size of deposited particles is as large as 2 μm (Fig. 3a), indicating the significant reaction of the gaseous Cr species from Cr_2O_3 with LSCF. For the LSCF sample heat-treated at 900°C in the presence of SO_2 for 48 h, there is a formation of large number of small (~80 nm) and large (~700 nm) particles and the formation of the particles appears to be random on both the grain boundaries and the

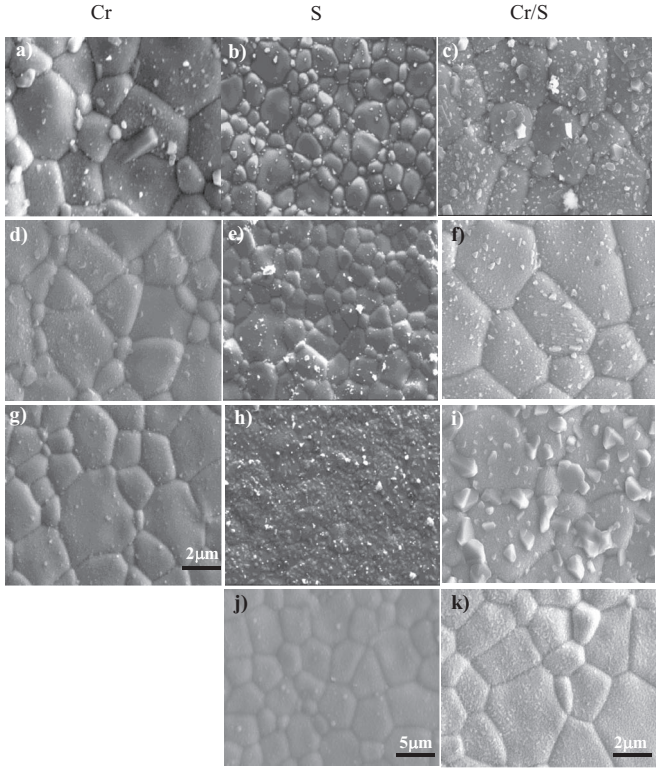

Figure 3. SEM micrographs of LSCF surface after heat-treatment for 48 h in the presence of Cr_2O_3 (Cr, left), 20 ppm SO_2 (S, middle) and Cr_2O_3 and 20 ppm SO_2 (Cr/S, right) at (a,b,c) 900°C, (d,e,f) 800°C, (g,h,i) 700°C, and (j,k) 600°C. The scale bar applies to the micrographs of the same column.

surface of LSCF grains (Fig. 3b). However, for the samples heat-treated at 900°C in the presence of Cr and S for 48 h, large number of deposited particles in the size ~1.0 μm were observed (Fig. 3c). Compared with the one in the presence of Cr or S (Fig. 3a and 3b), significantly more deposited particles were formed on the surface, which indicates the additive deposition effect of Cr and S on the surface of LSCF in the presence of both Cr and S contaminants.

In the case of the presence of Cr contaminant, the size and number of the deposits decrease rapidly with the decrease of temperature (Fig. 3d, 3g), indicating that the deposition rate of Cr species on the LSCF diminishes significantly with the temperature, as shown early.[17] The significant decrease in the Cr deposition on LSCF electrodes is mainly due to the fact that as the temperature decreases from 900°C to 700°C, both the partial pressure of gaseous chromium species and surface segregation of Sr decrease, thus significantly slowing the deposition process of chromium species. Significant deposition and formation of large and small particles were also observed for the LSCF bar sample heat-treated at 800°C in the presence of SO_2 (Fig. 3e). Very different from that observed for the Cr deposition, the most remarkable formation of deposited particles occurs on the LSCF electrodes after heat-treatment in the presence of SO_2 at 700°C (Fig. 3h). The surface of LSCF sample is almost completely covered by the deposits formed on the surface of LSCF grains and the particles formed are strontium sulfate, $SrSO_4$, as shown previously.[21] As the temperature decreases to 600°C, the sulfur deposition is substantially reduced with isolated deposits on the LSCF surface (Fig. 3j).

The deposition behavior in the presence of both Cr and S contaminants is very different from that observed in the presence of individual Cr or S. In the temperature range studied, the deposit formation on the surface of LSCF electrodes appears to be most significant at 900 and 700°C (Fig. 3c and 3i). The significant deposit formation for the reaction at 900°C is most likely dominated by the Cr deposition and this is supported by the prominent phase formation of $SrCrO_4$ (see Fig. 2). The substantial deposit formation also occurs on the LSCF electrodes at 700°C (Fig. 3i). However, the phase of the deposited particles is dominated by strontium sulfate, $SrSO_4$, rather than $SrCrO_4$ as detected by XRD (Fig. 2). It is in accordance with the severe sulfur poisoning effect on LSCF as a function of temperature.[21] Nevertheless, the size of the deposits formed on the surface of the LSCF electrode is in the range of 1~3.5 μm (Fig. 3i), very different from that formed in the presence of S only after the heat-treatment at the same temperatures (Fig. 3h). This may indicates the complex effect of the co-presence of Cr and S contaminants on the deposition and grain growth of the $SrSO_4$ dominated deposit phase. When the temperature decreased to 600°C, the numbers of the particles formed on the LSCF surface decreased substantially with numerous fine particles (35 nm) (Fig. 3k). This indicates the significantly reduced activity between LSCF and Cr+S at temperatures below 700°C.

Phase analysis of the deposits.— The formation of deposited particles on the surface of LSCF bar samples was further investigated using confocal Raman spectroscopy. Figure 4 is the optical microscopy images and Raman spectra of the LSCF surface after heat-treatment at 900°C and 800°C in the presence of Cr and S contaminants for 48 h. As shown in Figure 4g, the Raman spectra of the deposits on the LSCF surface with a wavelength of 865 cm^{-1} and 1000 cm^{-1} correspond to the phases of $SrCrO_4$[26] and $SrSO_4$.[27] From the Raman mapping image in Figure 4c–4f, it can be easily seen that isolated and large $SrCrO_4$ particles were formed on the LSCF surface at 900°C, while as the $SrCrO_4$ particles formed at 800°C were much smaller most likely due to the reduced partial pressure of gaseous Cr species. The reduction in operation temperature can significantly slow the deposition process of chromium species on LSCF cathodes. The detection of $SrSO_4$ phase by the Raman spectroscopy and not by XRD also indicates the high sensitivity of Raman spectroscopy techniques for the study of sulfur deposition. However, when the temperature decreased to 700°C, the Raman spectroscopy only detects the presence of $SrSO_4$ and no Raman shift signal associated with $SrCrO_4$ is observed (Fig. 5d), consistent with the XRD result. Raman image mapping with wavelength

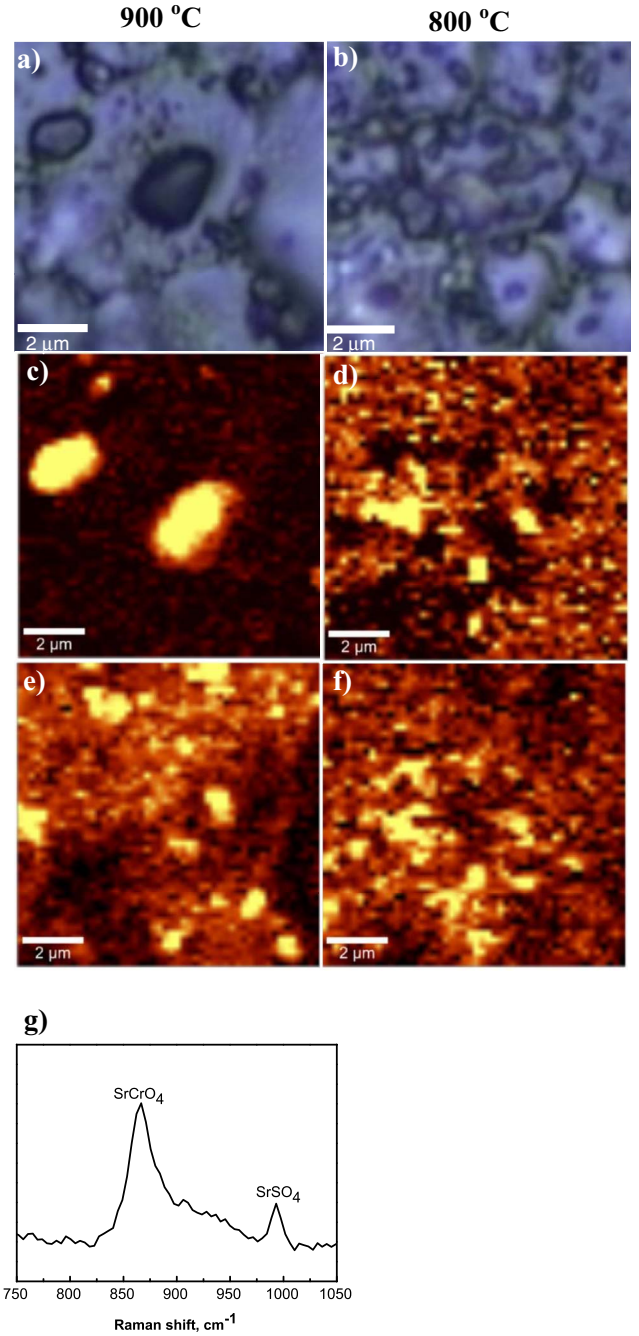

Figure 4. (a, b) Optical microscope images of LSCF surface after heat-treatment in the presence of Cr_2O_3 and 20 ppm SO_2; Raman mapping at wavelength of (c, d) 863 cm^{-1} corresponding to $SrCrO_4$ and (e, f) 1000 cm^{-1} corresponding to $SrSO_4$. Typical Raman spectra from corresponding areas at 900°C is given in (g).

of 1000 cm^{-1} shows the dominant formation of $SrSO_4$ phase (Fig. 5b). The results indicate that sulfur poisoning is dominant at lower temperatures (i.e., 700°C) with the formation of the $SrSO_4$ as the reaction products.

The composition and phase of the deposits on the LSCF surface was further investigated by XPS. Figure 6a shows the selected survey scan of the deposits on the LSCF surface after heat-treatment at 800°C, indicating the presence of Sr, Cr, S, La and O elements. The deconvolution of Sr $3d_{5/2\text{-}3/2}$ in LSCF generally shows that the Sr 3d peaks are mainly consisted of two distinctive peaks of $3d_{5/2}$ at lower binding energy (BE) ranges and $3d_{3/2}$ at relatively higher BE ranges[28]

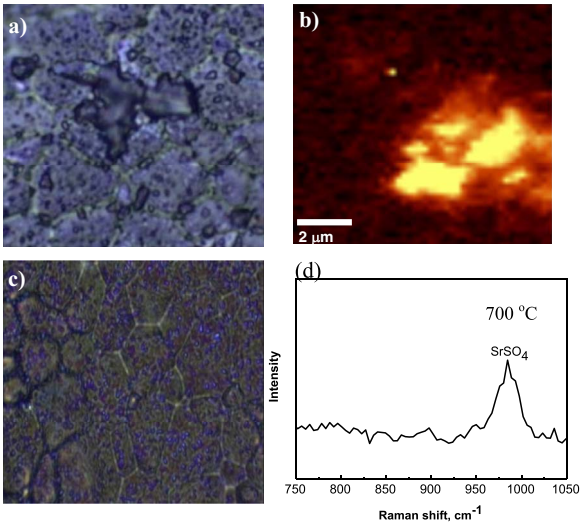

Figure 5. Optical microscope images of LSCF surface after heat-treatment at (a) 700°C and (c) 600°C in the presence of Cr_2O_3 and 20 ppm SO_2, (b) Raman mapping at wavelength of 1000 cm^{-1} corresponding to $SrSO_4$ and (d) Typical Raman spectra from selected areas of LSCF surface at 700°C. Scale bar applies to all graphs.

(see Fig. 6b). For the LSCF samples heat-treated at 900°C, deconvolution analysis indicates that Sr 3d spectrum is comprised of 4 peaks at 134.0 eV, 135.8 eV, 131.7 eV and 134.5 eV at, respectively. Based on the XPS data that the BE of Sr in SrO is 132.8 eV[29] and 133.8 eV in $SrCO_3$,[30] the main peaks in LSCF measured at 134.0 eV and 135.8 eV are originated from the $SrSO_4$ phase;[31] while the BE at 131.7 eV (Sr $3d_{5/2}$) and 134.5 eV (Sr $3d_{3/2}$) is correlated to the formation of the perovskite phase showing a charge state of Sr^{2+}.[32] At 800°C, the Sr 3d spectrum is similar to that measured at 900°C, comprised of peaks at 134.1 eV (Sr $3d_{5/2}$), 135.8 eV (Sr $3d_{3/2}$), 131.2 eV (Sr $3d_{5/2}$) and 132.9 eV (Sr $3d_{3/2}$). At 700°C, the Sr 3d spectrum is dominated by peaks at 134.3 eV (Sr $3d_{5/2}$) and 136.1 eV (Sr $3d_{3/2}$), and the peak intensity at 131.3 eV (Sr $3d_{5/2}$) and 133.0 eV (Sr $3d_{3/2}$) is relatively weak. At 600°C, the Sr 3d spectrum is mainly comprised of 2 peaks at 134.2 eV (Sr $3d_{5/2}$) and 135.9 eV (Sr $3d_{3/2}$).

In general, for each type of sulfur species, there is a doublet consisting of S $2p_{3/2}$ and S $2p_{1/2}$ (spin-orbit coupling) with the intensity ratio of 2:1.[33] The results show that the BE of the deconvoluted S $2p_{3/2}$ spectra is 168.5 eV, 168.6 eV, 169.2 eV and 168.7 eV at 900°C, 800°C, 700°C and 600°C, respectively (Fig. 6e), which is in accordance with the reported XPS results of $SrSO_4$.[31] The detection of the main peaks of Sr and S spectra associated with $SrSO_4$ indicates that deposition and formation of $SrSO_4$ phase occurs on the surface of LSCF at the temperature range in this study. This is in excellent agreement with the Raman spectroscopy results.

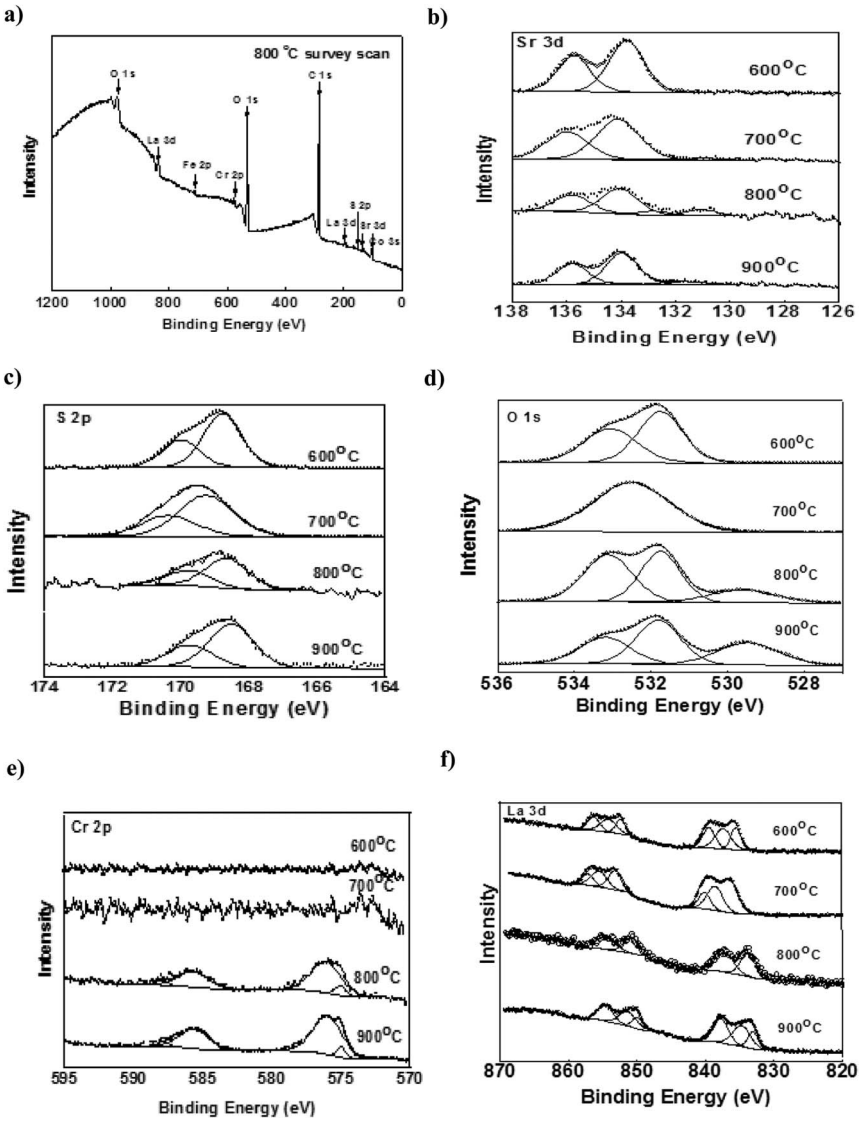

Figure 6. (a) typical XPS survey scan at 800°C and selected high resolution XPS of (b) Sr 3d, (c) S 2p, (d) O 1s, (e) Cr 2p and (f) La 3d of LSCF bar samples after heat-treatment at different temperatures and in the presence of Cr and S contaminants for 48 h.

Table I. Phase formation and analysis by XRD, XPS and Raman spectroscopy.

	900°C	800°C	700°C	600°C
		XRD		
$SrCrO_4$	√	√	nd	nd
$SrSO_4$	nd	nd	√	√
		Raman		
$SrCrO_4$	√	√	nd	nd
$SrSO_4$	√	√	√	nd
		XPS		
Cr(III)	√	√	nd	nd
$SrSO_4$	√	√	√	√
$La_2(SO_4)_3$	nd	nd	√	nd

*nd-not detected.

Various oxygen species of oxide materials can be identified with the BE differences. The O 1s peak, typical of perovskite materials, consists of three components at about 529, 531 and 532 eV which are usually attributed to lattice, surface, and adsorbed oxygen, respectively.[34] For the LSCF samples that were heat treated at 900°C and 800°C, the low BE (529.5–529.6 eV) of the deconvoluted O1s spectra is associated with the lattice oxygen; intermediate BE (531.7–531.8 eV) associated with surface oxygen; high BE (533.2–533.1 eV) with adsorbed oxygen. The high BE is related to the oxygen-containing species which occurs relatively near the surface and/or surface OH group caused by hydroxyl environment.[35–40] For the sample that was heat-treated at 700°C, the BE of the deconvoluted O1s spectra is 532.5 eV, which could be correlated to the adsorbed oxygen species or carbonate. At low temperature of 600°C, the BE of the deconvoluted O1s (531.7 eV, 533.1 eV) may correspond to the chemisorbed oxygen in the form of O^{2-} and the oxygen-containing species.

In the case of Cr 2p spectra measured at different temperatures, no obvious Cr 2p spectra was detected at 600°C and 700°C, meaning that the Cr deposition at temperatures equal to or below 700°C is not favorable. Cr 2p spectra were observed for the LSCF samples heat-treated at 900 and 800°C. After deconvolution, the BE of the Cr $2p_{1/2}$ is 585.6 eV and 585.7 eV at 900°C and 800°C, respectively, while the BE of the Cr $2p_{3/2}$ is 575.9 eV and 576.3 eV at 900°C and 800°C, respectively. This is consistent with the BE of 586.2–586.9 eV for Cr $2p_{1/2}$ and 576.4–577.0 eV for Cr $2p_{3/2}$ in Cr^{3+}-containing compounds.[41] However, it is difficult to identify BE of 588.1–589.1 eV for Cr $2p_{1/2}$ peak and 578.3–579.8 eV for Cr $2p_{3/2}$ peak associated with Cr^{6+} compounds. The XPS analysis data confirm the presence of Cr^{3+}, but not Cr^{6+} on the LSCF surface at 900 and 800°C. XPS technique provides both elemental and, to a certain extent, chemical information in the top 3–30 atomic layers (10–100 Å) of the samples. The dominant spectra associated with Cr^{3+} may indicate that surface of the Cr deposit particles is covered by Cr_2O_3 while the core is the $SrCrO_4$ as detected by XRD (Fig. 2).

The La $3d_{5/2}$ peak was observed at 833.0 eV for the sample heat-treated at 900°C, similar to the value of 833.8 eV for as-prepared sample,[42] and shifted to 834.1 eV, 836.3 eV and 835.4 eV as temperature decreased from 800°C to 600°C (Fig. 6f). The BE of the La $3d_{5/2}$ peaks agrees with that reported by Wu et al.[43] for $La_{0.5}Sr_{0.5}MnO_3$ pellets with a main line at 834.1 eV. The exposure at lower temperatures, especially 700°C, resulted a shift to a higher BE (836.3 eV), indicating the possible formation of $La_2(SO_4)_3$.[42]

Table I summarizes the phases formed on the surface of LSCF dense bar samples after heat-treatment in the presence of Cr and S at different temperatures, based on XRD, Raman and XPS analysis. The results indicate that in the presence of Cr and 20 ppm SO_2, the deposition and reaction products between LSCF and contaminants are dependent on the temperature: $SrCrO_4$ only forms at high temperature of 900 and 800°C, while $SrSO_4$ forms at the temperature ranges studied.

Oxygen surface exchange coefficient.— Figure 7 is the electrical conductivity relaxation profiles of LSCF samples measured at 900°C as a function of exposure time in the absence and presence of Cr, S and Cr/S. In the absence of contaminants, the initial relaxation time is around 400 s. The oxygen exchange coefficients, k_{chem} of

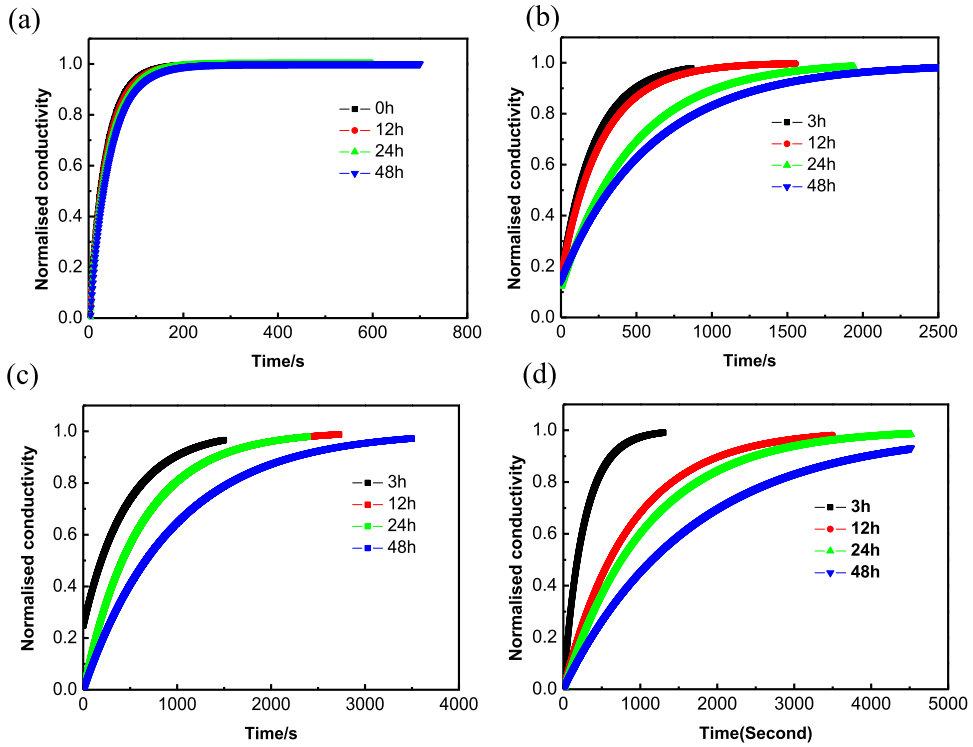

Figure 7. Comparison of electrical conductivity relaxation profiles of LSCF bar samples as a function of exposure time (a) in the absence of Cr+/ and in the presence of (b) Cr_2O_3, (c) 20 ppm SO_2 and (d) Cr/S at 900°C.

as-prepared LSCF measured is 6×10^{-3} cm s^{-1} at 900°C, respectively, and decreased slightly with the heat-treatment time. In the case of the ECR relaxation profiles of LSCF samples measured in the presence of contaminant, the relaxation time increased from 700 s to 2500 s after being exposed to Cr_2O_3 for 48 h at 900°C, while in the presence of 20 ppm SO_2, the relaxation time increased from 1500 s to 3500 s. However, the relaxation time increased from 1500 to 4500 s after being exposed to both Cr and S. The k_{chem} value is 1.5×10^{-4} cm s^{-1}, 9×10^{-5} cm s^{-1}, 5×10^{-5} cm s^{-1} at 900°C in the presence of Cr, S and Cr/S after exposed for 48 h, respectively. The results also show that the k_{chem} of LSCF after being exposed to the Cr and S at 900°C is two orders of magnitude lower than that of the freshly-prepared LSCF (6×10^{-3} cm s^{-1}). The deposition and formation of $SrCrO_4$ and $SrSO_4$ on the surface of LSCF cathode materials can lead to the significant reduction in k_{chem} for the O_2 reduction on LSCF electrodes, indicating that the co-presence of chromium and sulfur contaminants is significant detrimental to the electrocatalytic activity of LSCF cathodes of SOFCs.

Conclusions

The deposition and poisoning of the co-presence of chromium and sulfur contaminants were investigated on LSCF bar samples at temperature range of 900–600°C. SEM microstructure analysis indicates that the interaction between LSCF and chromium and sulfur contaminant species depends strongly on the temperature and deposit formation on the surface of LSCF surface is most significant at temperature of 700°C. XRD, Raman and XPS analysis demonstrated that in the presence of Cr and 20 ppm SO_2, the deposition and reaction products between LSCF and Cr/S contaminants are dependent on the temperature: $SrCrO_4$ only forms at high temperature of 900 and 800°C, while formation of $SrSO_4$ phase occurs at the temperature ranges tested in the present study. The k_{chem} value is 1.5×10^{-4} cm s^{-1}, 9×10^{-5} cm s^{-1}, 5×10^{-5} cm s^{-1} at 900°C in the presence of gaseous Cr, S and Cr/S, respectively. The results indicate that the co-presence of chromium and sulfur contaminants can cause the significant deposition and formation of $SrCrO_4$ and/or $SrSO_4$, which are detrimental to the oxygen exchange and surface diffusion process on the LSCF electrode materials.

Acknowledgment

The authors acknowledge the facilities, scientific and technical assistance of the Curtin University Scanning Probe Microscopy, Department of Chemistry/Nanochemistry Research Institute, Curtin University, a facility partially funded by the University, State and Commonwealth Governments. The authors also acknowledge the use of equipment, scientific and technical assistance of the WA X-Ray Surface Analysis Facility, funded by the Australian Research Council LIEF grant LE120100026.

References

1. X. Chen, L. Zhang, E. Liu, and S. P. Jiang, *International Journal of Hydrogen Energy*, **36**, 805 (2011).
2. H. Y. Tu and U. Stimming, *J. Power Sources*, **127**, 284 (2004).
3. J. W. Fergus, *International Journal of Hydrogen Energy*, **32**, 3664 (2007).
4. J. A. Schuler, C. Gehrig, Z. Wuillemin, A. J. Schuler, J. Wochele, C. Ludwig, A. Hessler-Wyser, and J. Van Herle, *Journal of Power Sources*, **196**, 7225 (2011).
5. T. Horita, H. Kishimoto, K. Yamaji, M. E. Brito, Y. P. Xiong, H. Yokokawa, Y. Hori, and I. Miyachi, *J. Power Sources*, **193**, 194 (2009).
6. K. F. Chen, N. Ai, L. Zhao, and S. P. Jiang, *J. Electrochem. Soc.*, **160**, F183 (2013).
7. K. F. Chen, N. Ai, L. Zhao, and S. P. Jiang, *J. Electrochem. Soc.*, **160**, F301 (2013).
8. S. P. Jiang and X. B. Chen, *Int. J. Hydrog. Energy*, **39**, 505 (2014).
9. S. P. Jiang, J. P. Zhang, L. Apateanu, and K. Foger, *Journal of The Electrochemical Society*, **147**, 4013 (2000).
10. S. P. Jiang, J. P. Zhang, and K. Foger, *Journal of The Electrochemical Society*, **148**, C447 (2001).
11. T. Horita, Y. P. Xiong, H. Kishimoto, K. Yamaji, M. E. Brito, and H. Yokokawa, *J. Electrochem. Soc.*, **157**, B614 (2010).
12. E. Konysheva, H. Penkalla, E. Wessel, J. Mertens, U. Seeling, L. Singheiser, and K. Hilpert, *J. Electrochem. Soc.*, **153**, A765 (2006).
13. Y. M. Kim, X. B. Chen, S. P. Jiang, and J. Bae, *J. Electrochem. Soc.*, **159**, B185 (2012).
14. S. P. Jiang, S. Zhang, and Y. D. Zhen, *J. Electrochem. Soc.*, **153**, A127 (2006).
15. L. Zhao, J. Drennan, C. Kong, S. Amarasinghe, and S. P. Jiang, *Journal of Materials Chemistry A*, **2**, 11114 (2014).
16. X. B. Chen, Y. D. Zhen, J. Li, and S. P. Jiang, *Int. J. Hydrog. Energy*, **35**, 2477 (2010).
17. C. C. Wang, T. Becker, K. F. Chen, L. Zhao, B. Wei, and S. P. Jiang, *Electrochim. Acta*, **139**, 173 (2014).
18. L. D. Emberson, M. R. Ashmore, F. Murray, J. C. I. Kuylenstierna, K. E. Percy, T. Izuta, Y. Zheng, H. Shimizu, B. H. Sheu, C. P. Liu, M. Agrawal, A. Wahid, N. M. Abdel-Latif, M. van Tienhoven, L. I. de Bauer, and M. Domingos, *Water Air and Soil Pollution*, **130**, 107 (2001).
19. F. Wang, K. Yamaji, D. H. Cho, T. Shimonosono, M. Nishi, H. Kishimoto, M. E. Brito, T. Horita, and H. Yokokawa, *Fuel Cells*, **13**, 520 (2013).
20. R.-R. Liu, S. Taniguchi, Y. Shiratori, K. Ito, and K. Sasaki, *ECS Transactions*, **35**, 2255 (2011).
21. C. C. Wang, K. F. Chen, and S. P. Jiang, *J. Electrochem. Soc.*, **161**, F1133 (2014).
22. J. A. Schuler, H. Yokokawa, C. F. Calderone, Q. Jeangros, Z. Wuillemin, A. Hessler-Wyser, and J. Van herle, *Journal of Power Sources*, **201**, 112 (2012).
23. J. A. Lane and J. A. Kilner, *Solid State Ionics*, **136**, 997 (2000).
24. T. Zhang, R. K. Brow, W. G. Fahrenholtz, and S. T. Reis, *Journal of Power Sources*, **205**, 301 (2012).
25. M. R. Bissengaliyeva, D. B. Gogol, S. T. Taimassova, N. S. Bekturganov, and A. T. Bort, *Thermochimica Acta*, **565**, 227 (2013).
26. Y.-H. Chen, E. Huang, and S.-C. Yu, *Solid State Communications*, **149**, 2050 (2009).
27. A. E. Hughes, S. Mayoa, Y. S. Yang, T. Markley, S. V. Smith, S. Sellaiyan, A. Uedono, S. G. Hardin, and T. H. Muster, *Progress in Organic Coatings*, **74**, 726 (2012).
28. Q. Liu, X. Dong, G. Xiao, F. Zhao, and F. Chen, *Adv Mater*, **22**, 5478 (2010).
29. M. I. Sosulnikov and Y. A. Teterin, *J Electron Spectrosc*, **59**, 111 (1992).
30. R. P. Vasquez, *Surf. Sci. Spectra*, **1**, 5 (1992).
31. C. D. Wagner AVN, A. Kraut-Vass, J. W. Allison, C. J. Powell, and J. R. Rumble, *NIST Standard Reference Database* 20, Version 3.4. (2003).
32. J. N. Kuhn and U. S. Ozkan, *Journal of Catalysis*, **253**, 200 (2008).
33. C. Guimon, A. Gervasini, and A. Auroux, *The Journal of Physical Chemistry B*, **105**, 10316 (2001).
34. F. Puleo, L. F. Liotta, V. L. Parola, D. Banerjee, A. Martorana, and A. Longo, *Physical chemistry chemical physics*, **16**, 22677 (2014).
35. M. I. Ivanovskaya, D. A. Kotikov, V. V. Pan'Kov, and V. V. Zyryanov, *Inorg Mater*, **45**, 910 (2009).
36. J. H. Kim, *Applied Surface Science*, **258**, 350 (2011).
37. A. C. Tavares, M. I. Da Silva Pereira, M. H. Mendonça, M. R. Nunes, F. M. Costa, and C. M. Sá, *Journal of Electroanalytical Chemistry*, **449**, 91 (1998).
38. M. Imamura, N. Matsubayashi, and H. Shimada, *Journal of Physical Chemistry B*, **104**, 7348 (2000).
39. P. Wang, L. Yao, M. Wang, and W. Wu, *Journal of Alloys and Compounds*, **311**, 53 (2000).
40. N. A. Merino, B. P. Barbero, P. Eloy, and L. E. Cadús, *Applied Surface Science*, **253**, 1489 (2006).
41. D. S. Chapin, J. A. Kafalas, and J. M. Honig, *The Journal of Physical Chemistry*, **69**, 1402 (1965).
42. E. D. Wachsman, Solid-state Ionic Devices II: Ceramic Sensors, in *Electrochemical Society Proceedings* p. 2 (2001).
43. Q.-H. Wu, M. Liu, and W. Jaegermann, *Mater Lett*, **59**, 1980 (2005).